

## **CAD on liver using CT and MRI**

Xuejun Zhang<sup>a</sup>, Hiroshi Fujita<sup>b</sup>, Takeshi Hara<sup>b</sup>, Xiangrong Zhou<sup>b</sup>, Masayuki Kanematsu<sup>c</sup>, Ryujiro Yokoyama<sup>c</sup>, Hiroshi Kondo<sup>c</sup>, and Hiroaki Hoshi<sup>c</sup>

<sup>a</sup>School of Computer, Electronics and Information, Department of Electronics and Information Engineering, Guangxi University, Nanning City, Guangxi 530004, P. R. China

<sup>b</sup>Department of Intelligent Image Information, Division of Regeneration and Advanced Medical Sciences, Graduate School of Medicine, Gifu University, Gifu 501-1194, Japan

<sup>c</sup>Department of Radiology, Gifu University School of Medicine & Gifu University Hospital, Gifu 501-1194, Japan

Email: xjzhang@gxu.edu.cn

**Abstract.** The incidence of liver diseases is very high in Asian countries. This paper introduces our computer-aided diagnosis (CAD) system for diagnosing liver cancer and describes the fundamental technologies employed in the system and its performance. The results showed that our system is useful for diagnosing liver cancer, and it is expected that employing CAD in clinical practice would reduce the mortality caused by liver cancer in Asian countries.

**Keywords:** Computer-aided diagnosis, Segmentation, Liver, Tumor, Cirrhosis, Multi-phase CT, Edge extraction, Subtraction method, Shape and texture analysis.

### **1 Introduction**

Primary malignant liver tumors, including hepatocellular carcinoma (HCC), cause 1.25 million deaths per year worldwide. HCC is prevalent in Asia and Africa because of presence of a large subclinical population with hepatitis C virus infection. Additionally, during the last 2 decades, the mortality rate from primary liver cancer is reported to have increased by 41%, and the proportion of hospitalization due to this disease has increased by 46% [1]. Although globally liver cancer is ranked 9 as a cause of death due to organ cancer, it is ranked from 1 to 3 in many Asian countries, particularly in the coastal regions such as Japan, Korea, China, and Southeast Asian countries. Early detection and accurate staging of liver cancer is an important issue in practical radiology. Currently, although multidetector-row computed tomography (MDCT) or MRI is widely used for the diagnosis of liver tumors, the amount of information obtained from CT/MRI is very large, and it is difficult for inexperienced radiologists or physicians to interpret all the images in a short duration.

The purpose of our study was to establish a computer-aided diagnosis (CAD) and surgery system for aiding decision-making with regard to the diagnosis of liver cancer or supporting radiologists and surgeons in planning of liver resections or living donor transplantation by using multiphase CT/MRI images.

2 CAD on liver using CT and MRI

## 2 Methods and Experimental Results

Three datasets from different hospitals were examined with different MDCT scanners. In the main dataset, an MDCT scanner (Aquilion; TOSHIBA, Japan) was used to scan a quadruple-phase protocol that included unenhanced, hepatic arterial, portal venous, and delayed phase images. Each patient received the contrast/bolus agent (Oypalomin370 or Optiray320) via a power injector at a rate of 3 ml/s, and the final average volume of the contrast material was 100 ml (range, 110–182 ml). Four complete acquisitions of the entire liver were obtained in a craniocaudal direction during one breath-hold with the following parameters: slice interval, 0.625–1.25 mm; bits stored, 16 bits; pixel-spacing, 0.50–0.625 mm; spatial resolution,  $512 \times 512$ ; 165 mAs; and 120 kVp. Non-contrast scanning (i.e., the first pass) was performed in all patients. The final average start time for the hepatic arterial phase was 37 s (range, 35–40 s). The portal venous phase and the equilibrium phase (i.e., the third and fourth passes, respectively) scans were acquired at 65 s (range, 60–70 s) and 180 s, respectively, after the contrast material injection. These cases were categorized by experienced radiologists, and 12 normal cases, 32 cases with 44 HCC tumors, and 9 other tumor cases were confirmed.

Precontrast T1-weighted MR images are ordinarily obtained by using a spin-echo or gradient-recalled-echo sequence. In our experiment, the repetition time (TR)/echo time (TE) was set at 316 ms/11 ms. Further, fast spin-echo (FSE) T2-weighted imaging, which has been shown to play a key role in the characterization of liver lesions, was performed by using an FSE sequence. The signal intensities of metastases using T1- and T2-weighted images are variable but are usually prolonged. T2-weighted imaging is reported to be very effective in enabling radiologists to differentiate between cavernous hemangiomas and metastases. In our experiment, the effective TR/effective TE of an FSE T2-weighted image was set at 4615 ms/80 ms. We obtained the gadolinium-enhanced hepatic arterial and equilibrium phase images by using a phased-array body multicoil with the following settings: TE, 1.6 ms; TR, 150 ms; flip angle,  $90^\circ$ ; matrix,  $512 \times 512$ ; and breath-hold acquisition, 26 s. Images were obtained after administering an antecubital intravenous bolus injection of 0.1 mmol/kg gadopentetate dimeglumine (Gd-DTPA) (Magnevist; Schering AG, Berlin, Germany), followed by flushing with 15 ml of sterile saline solution. The scan timing was 18 s and 3 min after initiation of the contrast injection. Using a 1.5-T superconducting magnet (Signa Horizon; GE Medical Systems, Milwaukee, WI), 320 MR images of 80 patients (4 images per patient) with focal liver lesions were obtained. These cases were diagnosed by 2 experienced radiologists, and a majority of these cases were pathologically confirmed by biopsy or surgery. Although it was impossible to diagnose all lesions pathologically, the remaining patients underwent angiography-assisted ultrasonography, CT, or follow-up MRI to confirm the diagnosis. We followed a stringent criterion for diagnosing malignancy and excluded cases in which the lesion size was very small.

Based on the above CT/MRI datasets, our developed systems contained the following components:

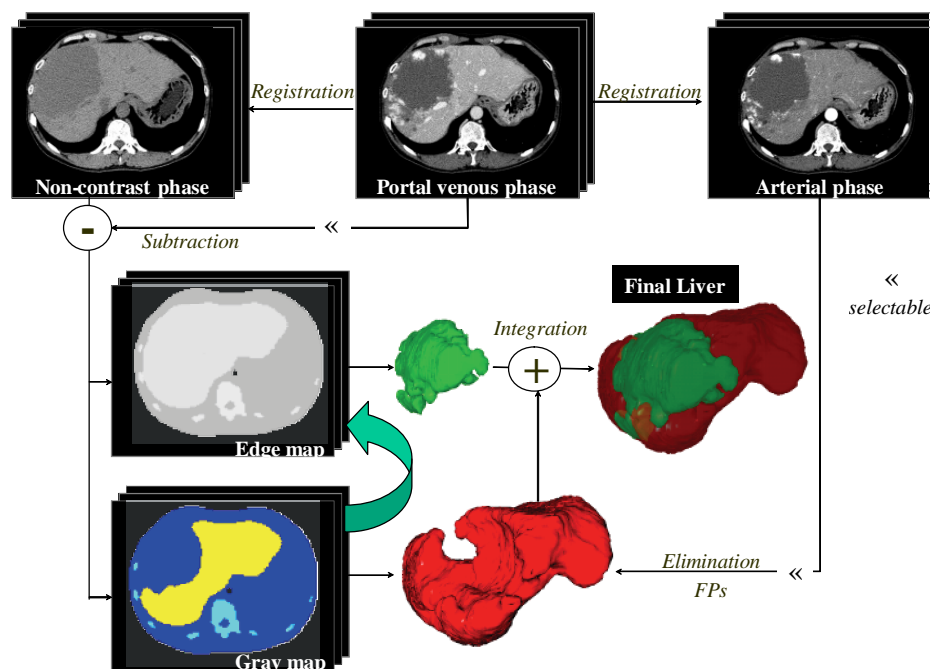


Fig. 1. An overall procedure of the segmentation of an abnormal liver region from MDCT based on the edge detection and subtraction method [2].

## 2.1 Segmentation of the liver region with tumor tissues

We propose a fully automatic method to segment the liver and other organs on multi-phase MRI or CT images, regardless of the presence of cirrhosis or tumors such as hemangioma, HCC or cyst within the liver [2]. Our method is based on the edge detection [3] or combined with a subtraction processing algorithm that is independent of the intensity or noise of the CT or MR images. In comparison to other methods [4–8], such a “Press-One-Button” system is extremely user-friendly and can be used without any training; moreover, it provides highly accurate 3D images of different organs within an average of 12 min of running on a PC (Pentium M 1.0 GHz with 512 MB RAM). This time is reasonable and acceptable for clinical applications. All the liver regions in 53 cases were successfully segmented by visual evaluation, without losing any part of the hepatic lesions. A comparison of the gold standard for liver regions prepared by radiologists with our experimental results revealed that in 6 cases of the entire dataset, the average error rate of liver segmentation was within 4.3%. Eleven hepatic tumors (3 hemangioma, 4 HCC, 3 metastasis, and 1 cyst) showing distinct intensity difference from the liver scanned in the portal venous MDCT images

#### 4 CAD on liver using CT and MRI

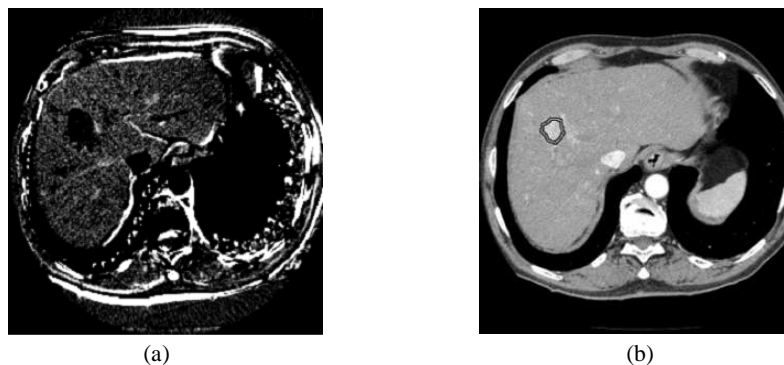


Fig. 2 Extraction of HCC candidates is performed by subtracting the equilibrium phase image from the arterial phase image. The edge of the HCC is lost in the subtraction map (a) after edge detection by Sobel filter and LoG filter, and the final region of HCC (b) is obtained by the region growing method on the extracted candidate regions [9].

were extracted successfully and integrated into the final region. Figure 1 shows an extracted 3D liver tissue, in which a large lesion that appears as a huge hole is of the region affected by hemangioma. Other cases as normal liver or HCC tumors with only subtle intensity difference to liver are preformed with high stable results by our proposed method without losing any hepatic tissues.

### 2.2 Computer-aided detection of hepatocellular carcinoma on multiphase CT images

Following the enhancement with the contrast material, the presence of HCC is indicated by high- and low-intensity regions in arterial and equilibrium phase images, respectively. We propose an automatic method for detecting HCC based on edge detection and subtraction processing [9]. Within a liver area segmented according to our scheme, black regions were selected by subtracting the equilibrium phase images with the corresponding registered arterial phase images. From these black regions, the HCC candidates were extracted as the areas without edges by using Sobel and LoG edge detection filters, as shown in Fig. 2a. The false-positive (FP) candidates were eliminated by using 6 features extracted from the cancerous and the surrounding liver regions. Other FPs were further eliminated by opening processing. Finally, an expansion process was applied to acquire the 3D shape of the HCC, as shown in Fig. 2b. In this experiment, we used the CT images of 44 patients with 44 HCCs. We successfully extracted 97.7% (43/44) HCCs successfully by our proposed method, with an average number of 2.1 FPs per case.

### 2.3 Application of an artificial neural network to the computer-aided differentiation of focal liver diseases in MR imaging

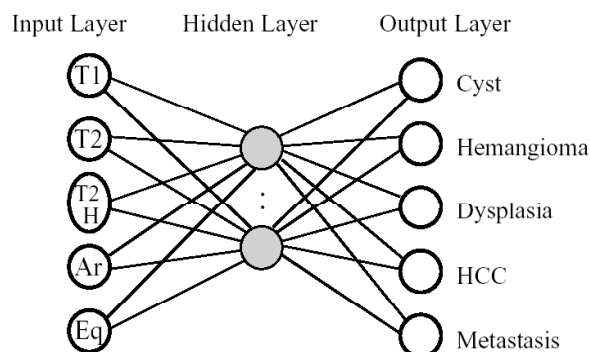


Fig. 3. A multi-layer feedforward network used in LiverANN [14-16] can automatically find out the internal relationship between inputs and outputs by learning from samples by employing backpropagation algorithm. Note: T2H = homogeneity of T2-weighted imaging. HCC = hepatocellular carcinoma.

The differentiation of focal liver lesions in MR imaging is primarily based on the intensity and homogeneity of lesions with different imaging sequences. However, in some patients, these imaging findings may be falsely interpreted due to the involved complexities. Our purpose was to establish a CAD system named LiverANN for classifying the pathologies of focal liver lesions into 5 categories by using the artificial neural network (ANN) technique, which has been proved to be useful in various medical fields [10-13]. On each MR image, a region of interest (ROI) in the focal liver lesion was delineated by a radiologist. The intensity and homogeneity within the ROI were automatically calculated to obtain numerical data that were analyzed by input signals to LiverANN. The outputs were the following 5 pathological categories of hepatic diseases, namely, hepatic cyst, hepatocellular carcinoma, dysplasia in cirrhosis, cavernous hemangioma, and metastasis. Of the 320 MR images obtained from 80 patients (4 images per patient) with liver lesions, LiverANN classified 50 cases of training set into 5 types of liver lesions with a training accuracy of 100% and 30 test cases with a testing accuracy of 93% [14-16].

#### 2.4 3D volume analysis of cirrhosis

Cirrhosis of the liver is one of the leading causes of death due to diseases, killing more than 12,000 people in Japan each year. In the United States, about 26,000 people die from chronic liver diseases and cirrhosis each year. Liver MR imaging is useful for the diagnosis of cirrhosis. The enlargement of the left lobe of the liver and the shrinkage of the right lobe are helpful signs in MR imaging in the diagnosis of cirrhosis of the liver [17-20]. To investigate whether the volume ratio of left-to-whole (LTW) is effective to differentiate a cirrhotic liver from a normal liver, we developed an automatic algorithm for segmentation and volume calculation of the liver region in MDCT scans and MR imaging [21]. As shown in Fig. 4a, the 3D liver is divided into

6 CAD on liver using CT and MRI

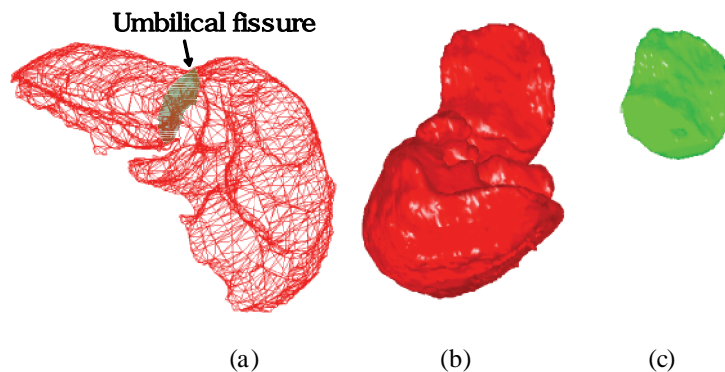


Fig. 4. 3D volume analysis of cirrhosis. (a) The liver is divided into left and right lobe by drawing an umbilical fissure. The volume ratio of LTW is defined as the ratio between the whole liver (b) and left lobe (c) volumes [21].

left and right lobes along the umbilical fissure. The volume ( $V$ ) of each part is calculated slice by slice. The degree of cirrhosis is defined as the ratio of  $LTW = V_{left}/(V_{right} + V_{left})$ , where  $V_{right} + V_{left}$  is the volume in Fig. 4b and  $V_{left}$  is the volume in Fig. 4c. 22 cases including normal and cirrhotic liver on MR and CT slices are used for 3D segmentation and visualization. The whole hepatic volume of the cirrhotic liver ( $931 \pm 307 \text{ cm}^3$ ) was slightly lower than that of the normal liver ( $1070 \pm 412 \text{ cm}^3$ ), while the volume of the left lobe in the cirrhotic liver ( $238 \pm 53 \text{ cm}^3$ ) was larger than that of the normal liver ( $176 \pm 69 \text{ cm}^3$ ). The volume ratio of LTW was relatively higher in the cirrhotic liver ( $25.6\% \pm 4.3\%$ ) than in the normal liver ( $16.4\% \pm 5.4\%$ ).

## 2.5 Improving the classification of the cirrhotic liver by shape and texture analysis

Two shape features were calculated from a segmented liver region, and 7 texture features were quantified using the grey level difference method (GLDM) [22] within the small ROIs. The degree of cirrhosis was derived by integrating the shape and texture features of the liver into a 3-layer feedforward ANN [23], as shown in Fig. 5. The liver was regarded as cirrhotic if the percentage of ROIs with a degree of cirrhosis of more than 0.5 was greater than 50%. The initial experimental result showed that the ANN-based method classified liver cirrhosis with a training accuracy of 100% on the 100 ROIs included in the training set. In the testing of the whole liver region, 82% (9/11) cirrhotic and 100% (7/7) normal cases were correctly differentiated from 18 test cases by using the shape and texture analysis as compared to 55% (6/11) cirrhotic and 100% (7/7) normal cases by using the texture analysis

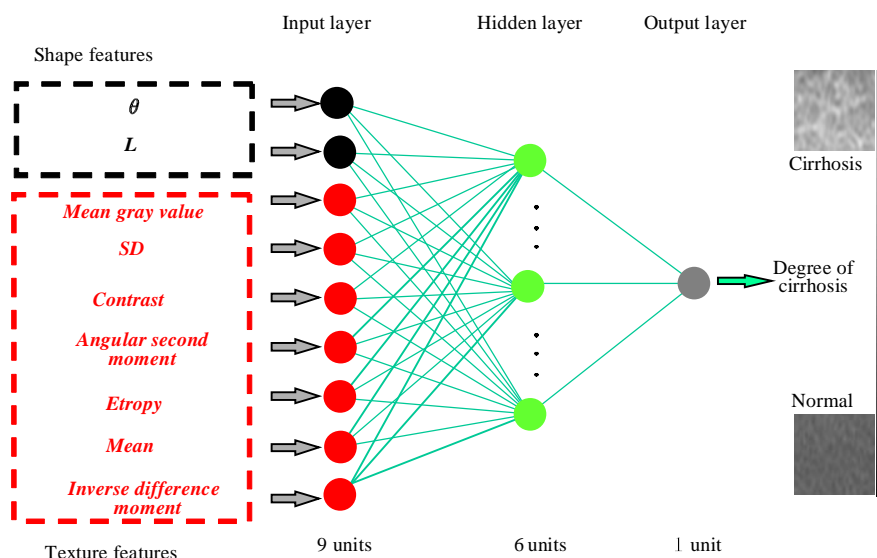


Fig. 5. ANN structure for calculating the degree of cirrhosis [24].

alone. According to the ROC analysis, the Az value (the area under the ROC curve) improved from 0.57 to 0.84 by integrating the shape features into ANN inputs [24].

### 3 Discussion

The challenge of a liver segmentation technique is to robustly extract the liver regions with lesions or regions that have received partial transplants. The liver not only has radiodensity that is similar to its surrounding structures, resulting in the common problem of connectivity to the heart, stomach, or kidney, but it is also affected by hepatic diseases that may change its shape and internal texture or homogeneity. In addition, the image quality from different modalities varies in terms of signal-to-noise ratio, motion artifacts, etc. There are some reports on the segmentation of the abdominal organs on CT images by using a thresholding method, likelihood function, or hepatic vessels. However, many reports address only the techniques involved in the segmentation of the normal liver tissues, and these techniques cannot usually be used for extracting the abnormal liver regions. In order to ensure that our software can be widely used in different hospitals for different modalities, we used edge detection in combination with a subtraction processing algorithm that is independent of the intensity or noise of the CT images or of the accuracy of the MR images.

Although our affine-based registration method was useful for liver segmentation, the position of cancer in arterial phase images might be different from that in equilibrium phase images when rigid transformation is used alone. In particular, if the

## 8 CAD on liver using CT and MRI

tumor is small in size, the subtraction process cannot enhance the cancer region in the same position. Therefore, the small HCC candidate was eliminated as FP after edge detection. In our study, this HCC could be detected by using the nonrigid transformation method [25, 26], even if the patient changed the duration of breath-hold frequently during the period when the scanning was performed twice.

Focal liver lesions can be accurately detected and characterized by MR imaging. The misdiagnosis by LiverANN might have occurred because some HCCs are mildly hyperintense in T2-weighted images, moderately hypervascular in the hepatic arterial phase, and hypointense in the equilibrium phase. Hypervascular metastases such as renal cell carcinoma or carcinoid tumor have brisk arterial enhancement and may be indistinguishable from HCC. The broad spectrum of enhancement pattern or morphology of HCC makes it difficult to characterize this type of tumor using the CAD algorithm, and some overlap in imaging features is observed between HCC and metastasis in daily clinical practice. Information of other features such as the presence of fibrous capsules or cirrhotic changes around the focal liver lesions, elevated serum alpha-fetoprotein (AFP) level, or history of extrahepatic primary cancer is critical in differentiating HCC and metastasis; such supplementary information other than signal intensity and homogeneity of lesions is very helpful to radiologists in correctly interpreting the MR images. The presence of cirrhosis and the patient's clinical and laboratory data are helpful in making the diagnosis. The integration of such additional information into LiverANN would be the next step of this study.

The results of our study showed that the left lobe of the liver was enlarged while the right lobe was shrunk in patients with liver cirrhosis. No statistically significant difference was observed in the whole hepatic volume between the cirrhotic liver and the normal liver. However, the difference in the volume ratio of LTW between the cirrhotic liver and the normal liver was significantly improved by our proposed method, and the 3D feature performed better than the 2D feature [27, 28].

The 2 misdiagnosed cirrhosis cases had very similar shape feature values to those of the normal cases; this is because the shape of the liver may change in different sleeping postures, and the shape features may be affected by the scanning position when only one 2D slice is used. Our next step is to calculate the 3D shape features to solve this problem, since the dullness of the left lobe remains the same regardless of the variation in the shape. Furthermore, the CAD system is expected to differentiate micronodular cirrhosis, macronodular cirrhosis, and mixed types into different categories by using ANN.

## 4 Conclusion

In conclusion, we developed a CAD system for the detection and diagnosis of liver diseases on MR and CT images. The experimental results demonstrated that our system functioning as a computer-aided differentiation tool may provide radiologists with referential opinion during the radiological diagnostic procedure; the performance

of our 3D segmentation technique was satisfactory for surgical use, and the agreement of the LTW ratio with shape and texture features may be effective for predicting cirrhosis on MR images. It is expected that employing CAD in clinical practice would reduce the mortality caused by liver cancer in Asian countries.

**Acknowledgments.** This research was supported in part by a Grant-in-Aid for Cancer Research from the Ministry of Health, Labour and Welfare, Japan, and in part by a Grant-in-Aid for Scientific Research from the Ministry of Education, Culture, Sports, Science and Technology, Japan. The authors would like to thank Gobert Lee, Hiroki Kato, Huiyan Jiang, Wenguang Li, Tetsuji Tajima, and Teruhiko Kitagawa for their assistance in a part of the LiverCAD project and Shigeru Nawanod and Kenji Shinozaki, who provided a part of the MDCT data used in this study.

## References

1. El-Serag, H. and Mason, A.: Rising incidence of hepatocellular carcinoma in the United States. *N. Engl. J. Med.* 340 (1999) 745–750
2. Zhang, X., Tajima, T., Kitagawa, T., Kanematsu, M., Zhou, X., Hara, T., Fujita, H., Yokoyama, R., Kondo, H., and Hoshi, H.: Segmentation of liver region with tumorous tissues. *Proc. of SPIE Medical Imaging 2007: Image Processing Vol.6512 (2007) 651235-1-651235-9*
3. Marr, D. and Hildreth, E.: Theory of edge detection. *Proc. Royal Society of London, B207, (1980) 187–217*
4. Hitosugi, T., Shimizu, A., Tamura, M., and Kobatake, H.: Development of a liver extraction method using a level set method and its performance evaluation. *Journal of Computer Aided Diagnosis of Medical Images 7 (2003) 1–9 (in Japanese)*
5. Gao, L., Heath, D., Kuszyk, B., and Fishman, E.: Automatic liver segmentation technique for three-dimensional visualization of CT data. *Radiology 201 (1996) 359–364*
6. Masumoto, J., Hori, M., and Sato, Y.: Automated liver segmentation using multislice CT images. *IEICE J84-D-II (2001) 2150–2161 (in Japanese)*
7. Bae, K., Giger, M., and Chen, C.: Automatic segmentation of liver structure in CT images. *Med. Phys. 20 (1993) 71–78*
8. Park, H., Bland, P.H., and Meyer, C.R.: Construction of an abdominal probabilistic atlas and its application in segmentation. *IEEE Trans. on Med. Imaging 22 (2003) 483–492*
9. Tajima, T., Zhang, X., Kitagawa, T., Kanematsu, M., Zhou, X., Hara, T., Fujita, H., Yokoyama, R., Kondo, H., and Hoshi, H.: Computer-aided detection (CAD) of hepatocellular carcinoma on multiphase CT images. *Proc. of SPIE Medical Imaging 2007: Computer-Aided Diagnosis Vol.6514 (2007) 65142Q-1-65142Q-10*
10. Asada, N., Doi, K., MacMahon, H., Montner, S.M., Giger, M.L., Abe, C., and Wu, Y.: Potential usefulness of an artificial neural network for differential diagnosis of interstitial lung disease: pilot study. *Radiology 177 (1990) 857–860*
11. Fujita, H., Katafuchi, T., Uehara, T. and Nishimura, T.: Application of artificial neural network to computer-aided diagnosis of coronary artery disease in myocardial SPECT bull's-eye images. *J. Nucl. Med. 33 (1992) 272–276*
12. Zhang, W., Doi, K., Giger, M.L., Nishikawa, R.M., and Schmidt, R.A.: An improved shift-invariant artificial neural network for computerized detection of clustered microcalcifications in digital mammograms. *Med. Phys. 23 (1996) 595–601*
13. Seki, K., Fujita, H., Hirako, K., Hara, T. and Ando, T.: Detection of microcalcifications on mammograms using neural networks. *Med. Imag. Tech. 15 (1997) 639–651 (in Japanese)*

10 CAD on liver using CT and MRI

14. Zhang, X., Kanematsu, M., Fujita, H., Hara, T., and Hoshi, H.: Computerized classification of liver disease in MRI using artificial neural network. Proc. of SPIE-Medical Imaging 2001: Image Processing 4322 (2001) 1735-1742
15. Kako, N., Zhang, X., Kanematsu, M., Fujita, H., Hara, T., and Li, W.: Study of computer-aided diagnosis on MR imaging. Radiology 255 (2002) 749 (abstract)
16. Kako, N., Zhang, X., Li, W., Kanematsu, M., Fujita, H., and Hara, T.: Artificial neural network method for differentiation of focal liver disease in MR imaging. Radiology 255 (2002) 646 (abstract)
17. Ito, K. and Mitchell, D.G.: Hepatic morphologic changes in cirrhosis: MR imaging findings. Abdom. Imag. 25 (2000) 456-461
18. Harbin, W.P., Robert, N.J., and Ferrucci, J.T.: Diagnosis of cirrhosis based on regional changes in hepatic morphology: A radiological and pathological analysis. Radiology 135 (1980) 273-283
19. Torres, W.E., Whitmire, L.F., and Gedgaudas, M.K.: Computed tomography of hepatic morphologic changes in cirrhosis of the liver. J. Comput. Assist. Tomogr. 11 (1986) 47-50
20. McNeal, C.R., Maynard, W.H., Branch, R.A., Powers, T.A., Arns, P.A., Gunter, K., Fitzpatrick, J.M., and Partain, C.L.: Liver volume measurements and three-dimensional display from MR images. Radiology 169 (1988) 851-864
21. Zhang, X., Li, W., Fujita, H., Kanematsu, M., Hara, T., Zhou, X., Kondo, H., and Hoshi, H.: Automatic segmentation of hepatic tissue and 3D volume analysis of cirrhosis in multi-detector row CT scans and MR imaging. IEICE Trans. Inf. & Syst. E87-D (8) (2004) 2138-2147
22. Haralick, R.M., Shanmugam, K. and Dinstein, I.: Texture features for image classification. IEEE Trans. Syst., Man, Cybern. SMC-3 (1973) 610-621
23. Rumelhart, D.E. and McClelland, J.L.: Learning representations by back-propagating errors. Nature. 323 (1986) 533-536
24. Zhang, X., Fujita, H., Kanematsu, M., Zhou, X., Hara, T., Kato, H., Yokoyama, R., and Hoshi, H.: Improving the classification of cirrhotic liver by using texture features, Proc. of the 2005 IEEE-EMBS (Engineering in Medicine and Biology), (2005) 867-870
25. Bookstein, F. L.: Principal warps: Thin-plate splines and the decomposition of deformations. IEEE Trans. on Pattern Analysis and Machine Intelligence. 11 (1989) 567-585
26. Wells, W., Viola, P.I., Atsumi, H., Nakajima, S., and Kikinis, R.: Multi-modal volume registration by maximization of mutual information. Med. Image Anal. 1 (1996) 35-51
27. Awaya, H., Mitchell, D. and Kamishima, T.: Cirrhosis: Modified caudate-right lobe ratio. Radiology 224 (2002) 769-774
28. Wang, Y., Itoh, K., Taniguchi, N., Toei, H., Kawai, F., Nakamura, M., Omoto, K., Yokota, K., and Ono, T.: Studies on tissue characterization by texture analysis with co-occurrence matrix method using ultrasonography and CT imaging. J. Med. Ultrasonics 26 (1999) 825-837